INTERNATIONAL JOURNAL FOR NUMERICAL METHODS IN FLUIDS
*Int. J. Numer. Meth. Fluids* 2006; **51**:285–304
Published online 17 November 2005 in Wiley InterScience (www.interscience.wiley.com). DOI: 10.1002/fld.1123

# Modelling turbulent swirling flows based on the algebraic two-equation ($K$–$\varepsilon$) approach

Yu-Ning Huang[1], Hui-Yang Ma[2,*,†] and Hong-Jie Chu[2]

[1]*State Key Laboratory for Turbulence and Complex Systems, Department of Mechanics and Engineering Science, Peking University, Beijing 100871, People's Republic of China*
[2]*Department of Physics, Graduate University of the Chinese Academy of Sciences, P.O. Box 3908, Beijing 100049, People's Republic of China*

SUMMARY

We investigate the principal aspects of modelling the fully-developed turbulent swirling flows based on the algebraic two-equation ($K$–$\varepsilon$) modelling approach. As a typical example, the characteristics of modelling the turbulent swirling flow in an axially rotating pipe based on the non-linear cubic $K$–$\varepsilon$ models of Craft *et al.* (*Int. J. Heat Fluid Flow* 1996; **17**:108–115), Shih *et al.* (*Proceedings of 11th Symposium on Turbulent Shear Flows*, Grenoble, France, 1997; 31.1–31.6), and Huang and Ma (*Phys. Rev. E* 2004; **70**:036302) are analysed and discussed in detail. Moreover, we carry out the numerical simulations by using the above three cubic models for the turbulent swirling flows in an axially rotating pipe and in an axisymmetric chamber, respectively, in comparison with the experimental data concerned. The numerical results indicate that, in addition to the frame-indifferent mean stretching tensor (the mean strain-rate tensor), the frame-dependent mean spin tensor actually plays an effective and important role as well in predicting the turbulent swirling flows. Copyright © 2005 John Wiley & Sons, Ltd.

KEY WORDS: turbulent swirling flows; rotation effects; cubic $K$–$\varepsilon$ models; mean spin tensor

## 1. INTRODUCTION

Turbulent swirling flows pose a challenging problem of practical importance, which, as has been well documented in the literature of turbulence modelling, is mainly due to the difficulty in predicting the rotation effects. For example, the fully-developed turbulent flow in an axially rotating pipe, a typical turbulent swirling flow, is one of the benchmark test cases for assessing the performance of any newly proposed turbulence closure model in predicting the complex

*Correspondence to: H.-Y. Ma, Department of Physics, Graduate University of the Chinese Academy of Sciences, P.O. Box 3908, Beijing 100049, People's Republic of China.
†E-mail: hyma@163bj.com

Contract/grant sponsor: National Natural Science Foundation of China; contract/grant number: 90205002

*Received 30 January 2005*
*Revised 3 September 2005*
*Accepted 5 September 2005*

turbulent flows. Over the past two decades, a number of important works on this interesting and challenging problem have been conducted, experimentally, for instance, by Murakami and Kikuyama [1], Kikuyama *et al.* [2], Anwer and So [3], Reich and Beer [4], Kitoh [5], Imao *et al.* [6] and, recently, in numerical calculations, by Malin and Younis [7], Shih *et al.* [8], Pettersson *et al.* [9], Speziale *et al.* [10], Wallin and Johansson [11], among others—in particular, Orlandi and Fatica [12] carried out the direct numerical simulations. The turbulent swirling flow through a straight pipe, even in a fully-developed state, is in fact a rather complex flow—its prediction, due to the prevalent rotation effects induced by the rotating pipe, proves to be very complicated and involved. Recently, it has been reported by Shih *et al.* [8] that even though some quadratic $K$–$\varepsilon$ models that satisfy the realizability and work quite successfully for some complex turbulent flows with separation, e.g. the quadratic model of Shih *et al.* [13], they are not able to capture the rotation effect of the mean swirl velocity. Indeed, the weakness of the linear eddy-viscosity $K$–$\varepsilon$ model, as pointed out by Launder [14], cannot be rectified by simply introducing quadratic terms to the modelling of the Reynolds stress. By contrast, the second-order (moment) closure models can predict the rotation effect of the mean swirl velocity, though they are computationally costly and in some cases even far from being accurate as shown in comparison with the experimental data (see, e.g. References [7, 9]). Generally speaking, in order to capture the rotation effects of the turbulent swirling flows based on the algebraic two-equation ($K$–$\varepsilon$) modelling approach, one has to resort to a cubic model, e.g. the model of Craft *et al.* [15] and the model of Shih *et al.* [8].

In this work, first, we shall analyse the principal aspects of modelling the fully-developed turbulent flow in an axially rotating circular pipe based on the algebraic two-equation ($K$–$\varepsilon$) modelling approach. The characteristics of modelling this typical turbulent swirling flow based on the non-linear cubic $K$–$\varepsilon$ models of Craft *et al.* [15] and Shih *et al*. [8], and the non-linear cubic $K$–$\varepsilon$ model recently developed by Huang and Ma [16] will be discussed in detail. It is shown that the fully-developed turbulent flow in an axially rotating pipe is by nature a *two-point boundary value problem* and its modelling necessarily requires the contributions from the cubic terms in a non-linear $K$–$\varepsilon$ model. In fact, all the previously proposed linear and non-linear quadratic $K$–$\varepsilon$ models, e.g. the standard $K$–$\varepsilon$ model, the linear $K$–$\varepsilon$ model of Yoshizawa and Nisizima [17], the quadratic $K$–$\varepsilon$ model of Speziale [18], the quadratic $K$–$\varepsilon$ model of Shih *et al.* [13], and the quadratic $K$–$\varepsilon$ model developed in Reference [19] as an illustrative example to exemplify a general approach to modelling the Reynolds stress, are incapable of capturing the rotation effects of the mean swirl velocity—actually, they all predict a solid-body-rotation mean swirl velocity profile, in contrast to the experimental results. However, it is shown that any cubic term in a non-linear model will combine the preceding linear terms, as a joint effort, to predict the rotation effect of the mean swirl velocity. The numerical results for the mean swirl (circumferential) velocity, the mean axial velocity, and the Reynolds stresses using the afore-mentioned three cubic models [8, 15, 16] are presented in comparison with the experimental data of Imao *et al.* [6]. Moreover, to further assess the performance of these three cubic models in predicting the turbulent swirling flow in an axisymmetric chamber, we shall carry out numerical simulations and make a comparison with the experimental results of Ahmed and Nejad [20]. The numerical results for these two typical turbulent swirling flows indicate that, in addition to the mean stretching tensor (the mean strain-rate tensor), the mean spin tensor actually plays an effective role as well in predicting the turbulent swirling flows.

 

## 2. ASPECTS OF MODELLING THE FULLY-DEVELOPED TURBULENT FLOW IN AN AXIALLY ROTATING PIPE

For a fully-developed turbulent flow of an incompressible Newtonian fluid in an axially rotating circular pipe, in which case the mean velocity field $\mathbf{U} = U_\theta(r)\mathbf{e}_\theta + U_z(r)\mathbf{e}_z$ and the angular velocity of the rotating pipe $\boldsymbol{\Omega} = \Omega\mathbf{e}_z$, where $\Omega = \text{const.}$, in cylindrical coordinates $(r, \theta, z)$ (note that $U_r = 0$ is a direct consequence of the continuity equation), the ensemble-averaged Navier–Stokes equations simplify to

$$-\frac{\partial \bar{P}}{\partial z} + \nu\nabla^2 U_z - \frac{\mathrm{d}\tau_{rz}}{\mathrm{d}r} - \frac{1}{r}\tau_{rz} = 0 \tag{1}$$

$$\nu\left(\nabla^2 U_\theta - \frac{U_\theta}{r^2}\right) - \frac{\mathrm{d}\tau_{r\theta}}{\mathrm{d}r} - \frac{2}{r}\tau_{r\theta} = 0 \tag{2}$$

where $\bar{P}$ is the modified mean pressure containing the body force potential (note that here $\partial\bar{P}/\partial z = \text{const.}$), $\nu$ is the kinematic viscosity, and the Laplacian simplifies to

$$\nabla^2 = \frac{1}{r}\frac{\mathrm{d}}{\mathrm{d}r}\left(r\frac{\mathrm{d}}{\mathrm{d}r}\right)$$

By rearrangement and integration, Equation (2) becomes

$$\nu\frac{\mathrm{d}}{\mathrm{d}r}\left(\frac{U_\theta}{r}\right) = \frac{\tau_{r\theta}}{r} \tag{3}$$

The Reynolds stress tensor $\boldsymbol{\tau}$ in cylindrical coordinates reads as follows:

$$(\boldsymbol{\tau}) = \begin{pmatrix} \tau_{rr} & \tau_{r\theta} & \tau_{rz} \\ \tau_{\theta r} & \tau_{\theta\theta} & \tau_{\theta z} \\ \tau_{zr} & \tau_{z\theta} & \tau_{zz} \end{pmatrix} \tag{4}$$

Clearly, given the constitutive equations for $\tau_{r\theta}$ and $\tau_{rx}$, say, an algebraic two-equation ($K$–$\varepsilon$) model, then Equations (1) and (3), in conjunction of the conventional $K$ and $\varepsilon$ equations, constitute in fact a *two-point boundary value problem*.

In this case, the mean stretching tensor $\mathbf{D} = \frac{1}{2}[\text{grad}\,\mathbf{U} + (\text{grad}\,\mathbf{U})^{\mathrm{T}}]$ and the mean spin tensor $\mathbf{W} = \frac{1}{2}[\text{grad}\,\mathbf{U} - (\text{grad}\,\mathbf{U})^{\mathrm{T}}]$ are as follows in physical components:

$$(\mathbf{D}) = \begin{pmatrix} 0 & \frac{1}{2}\left(\frac{\mathrm{d}U_\theta}{\mathrm{d}r} - \frac{U_\theta}{r}\right) & \frac{1}{2}\frac{\mathrm{d}U_z}{\mathrm{d}r} \\ \frac{1}{2}\left(\frac{\mathrm{d}U_\theta}{\mathrm{d}r} - \frac{U_\theta}{r}\right) & 0 & 0 \\ \frac{1}{2}\frac{\mathrm{d}U_z}{\mathrm{d}r} & 0 & 0 \end{pmatrix} \tag{5}$$

 

and

$$(\mathbf{W}) = \begin{pmatrix} 0 & -\frac{1}{2}\left(\frac{\mathrm{d}U_\theta}{\mathrm{d}r} + \frac{U_\theta}{r}\right) & -\frac{1}{2}\frac{\mathrm{d}U_z}{\mathrm{d}r} \\ \frac{1}{2}\left(\frac{\mathrm{d}U_\theta}{\mathrm{d}r} + \frac{U_\theta}{r}\right) & 0 & 0 \\ \frac{1}{2}\frac{\mathrm{d}U_z}{\mathrm{d}r} & 0 & 0 \end{pmatrix} \tag{6}$$

It has been reported in the literature that the standard $K$–$\varepsilon$ model fails to capture the rotation effects of the swirling flow, producing a solid-body-rotation mean circumferential (swirl) velocity $U_\theta$, which is inconsistent with the experimental results. In fact, it can be shown that all the linear $K$–$\varepsilon$ models and the previously proposed non-linear quadratic $K$–$\varepsilon$ models predict the same solid-body-rotation mean swirl velocity $U_\theta$ as does the standard $K$–$\varepsilon$ model. Here, without loss of generality, let us consider two linear and three non-linear (quadratic) $K$–$\varepsilon$ models, for example, to see the fact.

(1) The standard $K$–$\varepsilon$ model (SKE) (see Reference [21]):

$$\boldsymbol{\tau} = \frac{2K}{3}\mathbf{1} - 2C_\mu\frac{K^2}{\varepsilon}\mathbf{D} \tag{7}$$

where $C_\mu = 0.09$, and $\mathbf{1}$ denotes the unit tensor hereinafter.

(2) The linear $K$–$\varepsilon$ model of Yoshizawa and Nisizima [17]:

$$\boldsymbol{\tau} = \frac{2K}{3}\mathbf{1} - \frac{2v_t}{1 + C_{G1}(K/\varepsilon)(D/Dt)\ln v_t}\mathbf{D} \tag{8}$$

where $v_t = C_\mu K^2/\varepsilon$, $C_\mu = 0.09$, and $C_{G1} = 1.3$.

(3) The non-linear quadratic $K$–$\varepsilon$ model of Speziale [18]:

$$\boldsymbol{\tau} = \frac{2K}{3}\mathbf{1} - 2C_\mu\frac{K^2}{\varepsilon}\mathbf{D} + 4C_D C_\mu^2\frac{K^3}{\varepsilon^2}\left[\mathbf{D}^2 - \frac{1}{3}\mathrm{tr}(\mathbf{D}^2)\mathbf{1}\right] + 4C_E C_\mu^2\frac{K^3}{\varepsilon^2}\left[\overset{\diamond}{\mathbf{D}} - \frac{1}{3}\mathrm{tr}(\overset{\diamond}{\mathbf{D}})\mathbf{1}\right] \tag{9}$$

where $C_\mu = 0.09$, $C_D = C_E = 1.68$, and $\overset{\diamond}{\mathbf{D}} = (D/Dt)\mathbf{D} - (\mathrm{grad}\,\bar{\mathbf{v}})\mathbf{D} - \mathbf{D}(\mathrm{grad}\,\bar{\mathbf{v}})^{\mathrm{T}}$ is the Oldroyd derivative of $\mathbf{D}$.

(4) The non-linear quadratic $K$–$\varepsilon$ model of Shih *et al.* [13]:

$$\boldsymbol{\tau} = \frac{2K}{3}\mathbf{1} - 2C_\mu^*\frac{K^2}{\varepsilon}\mathbf{D} - \beta_2\frac{K^3}{\varepsilon^2}[\mathbf{WD} - \mathbf{DW}] \tag{10}$$

where

$$C_\mu^* = \frac{1}{A_0 + A_s^* U^*(K/\varepsilon)} \quad \text{and} \quad \beta_2 = \frac{2\sqrt{1 - 9C_\mu^{*2}\,\mathrm{tr}(\mathbf{D}^2)(K/\varepsilon)^2}}{1 + 6\sqrt{-\mathrm{tr}(\mathbf{D}^2)\,\mathrm{tr}(\mathbf{W}^2)(K/\varepsilon)^2}}$$

in which $A_0 = 6.5$, $A_s^* = \sqrt{6}\cos\phi$, $\phi = \frac{1}{3}\arccos(\sqrt{6}\,\mathrm{tr}(\mathbf{D}^3)/[\mathrm{tr}(\mathbf{D}^2)]^{3/2})$, and the shear parameter $U^* = \sqrt{\mathrm{tr}(\mathbf{D}^2) - \mathrm{tr}(\mathbf{W}^2)}$.

 

(5) A non-linear quadratic $K$–$\varepsilon$ model given in Reference [19]:

$$\boldsymbol{\tau} = \frac{2K}{3}\mathbf{1} - 2C_\mu \frac{K^2}{\varepsilon}\mathbf{D} + \gamma_1 C_\mu^2 \frac{K^3}{\varepsilon^2}\left[\mathbf{D}^2 - \frac{1}{3}\mathrm{tr}(\mathbf{D}^2)\mathbf{1}\right] - \gamma_2 C_\mu^2 \frac{K^3}{\varepsilon^2}\overset{\circ}{\mathbf{D}}$$

$$- \gamma_3 C_\mu \frac{K^2}{\varepsilon^3}(K\dot{\varepsilon} - 2\dot{K}\varepsilon)\mathbf{D} \tag{11}$$

where $C_\mu = 0.09$, $\gamma_1 = 2.896$, $\gamma_2 = 2.784$, and $\gamma_3 = 0.843$.

In this turbulent swirling flow, the above five models actually give the same form for $\tau_{r\theta}$, viz.

$$\tau_{r\theta} = -2\nu_T D_{r\theta} \tag{12}$$

where $\nu_T$ is the turbulent (eddy) viscosity, which changes from one model to another as seen.

For the standard $K$–$\varepsilon$ model:

$$-2\nu_T = -2C_\mu \frac{K^2}{\varepsilon} \tag{13}$$

For the linear $K$–$\varepsilon$ model of Yoshizawa and Nisizima [17]:

$$-2\nu_T = \frac{2\nu_t}{1 + C_{G1}(K/\varepsilon)(D/Dt)\ln \nu_t} \tag{14}$$

For the non-linear quadratic $K$–$\varepsilon$ model of Speziale [18]:

$$-2\nu_T = -2C_\mu \frac{K^2}{\varepsilon} \tag{15}$$

For the non-linear quadratic $K$–$\varepsilon$ model of Shih, Zhu, and Lumley (SZL) [13]:

$$-2\nu_T = -2C_\mu^* \frac{K^2}{\varepsilon} \tag{16}$$

And, for the non-linear quadratic $K$–$\varepsilon$ model of Huang [19]:

$$-2\nu_T = -2C_\mu \frac{K^2}{\varepsilon} - \gamma_3 C_\mu \frac{K^2}{\varepsilon^3}(K\dot{\varepsilon} - 2\dot{K}\varepsilon) \tag{17}$$

Therefore, noting that $D_{r\theta} = \frac{1}{2}r(\mathrm{d}/\mathrm{d}r)(U_\theta/r)$, substituting Equation (12) into Equation (3) thus gives

$$(\nu + \nu_T)\frac{\mathrm{d}}{\mathrm{d}r}\left(\frac{U_\theta}{r}\right) = 0 \tag{18}$$

Equation (18), together with the no-slip boundary condition, $U_\theta(r)|_{r=R} = R\Omega$, readily yields

$$U_\theta = r\Omega \tag{19}$$

namely, a solid-body-rotation mean swirl velocity $U_\theta$, which, however, is in contradiction to the experimental and the DNS results (see, e.g. References [6, 12]).

 

Thus, it is clear that, in contrast to the second-moment closure models based on modelling the Reynolds stress transport equation, which as shown are capable of predicting the mean swirl velocity's rotation effect, e.g. the model of Fu *et al.* [22] (see also Reference [7]), in the algebraic two-equation ($K$–$\varepsilon$) modelling approach, one has to resort to the non-linear cubic $K$–$\varepsilon$ models in order to predict the rotation effects and better describe the mean swirl velocity $U_\theta$ in an axially rotating turbulent pipe flow. In the following, we shall use the non-linear cubic $K$–$\varepsilon$ model of Craft *et al.* [15], the non-linear cubic $K$–$\varepsilon$ model of Shih *et al.* [8], and the non-linear cubic $K$–$\varepsilon$ model recently developed by Huang and Ma [16], respectively, to carry out the numerical simulations and compare the results in detail with the experiments.

To this end, we shall first analyse the characteristics of these three models in predicting the mean swirl velocity $U_\theta$ in axially rotating turbulent pipe flow—namely, the detailed features of $\tau_{r\theta}$ given by each model, which plays a key role in predicting the rotation effects on $U_\theta$ as shown in Equation (3). Now, let us consider:

(6) The non-linear cubic $K$–$\varepsilon$ model of Craft *et al.* (CLS) [15]:

$$\begin{aligned}\boldsymbol{\tau} = {} & \frac{2K}{3}\mathbf{1} - 2\tilde{C}_\mu\frac{K^2}{\varepsilon}\mathbf{D} + \beta_1\frac{K^3}{\varepsilon^2}\left[\mathbf{D}^2 - \frac{1}{3}\mathrm{tr}(\mathbf{D}^2)\mathbf{1}\right] + \beta_2\frac{K^3}{\varepsilon^2}(\mathbf{WD} - \mathbf{DW}) \\ & + \beta_3\frac{K^3}{\varepsilon^2}\left[\mathbf{W}^2 - \frac{1}{3}\mathrm{tr}(\mathbf{W}^2)\mathbf{1}\right] - \gamma_1\frac{K^4}{\varepsilon^3}\mathrm{tr}(\mathbf{D}^2)\mathbf{D} - \gamma_2\frac{K^4}{\varepsilon^3}\mathrm{tr}(\mathbf{W}^2)\mathbf{D} \\ & - \gamma_3\frac{K^4}{\varepsilon^3}\left[\mathbf{W}^2\mathbf{D} + \mathbf{D}\mathbf{W}^2 - \frac{2}{3}\mathrm{tr}(\mathbf{W}^2\mathbf{D})\mathbf{1}\right] - \gamma_4\frac{K^4}{\varepsilon^3}(\mathbf{WD}^2 - \mathbf{D}^2\mathbf{W}) \end{aligned} \tag{20}$$

where

$$\tilde{C}_\mu = \frac{0.3(1 - \exp[-0.36/\exp(-0.75\eta)])}{1 + 0.35\eta^{3/2}}, \quad \eta = \max(\tilde{S}, \tilde{\Omega})$$

in which

$$\tilde{S} = (K/\varepsilon)[2\mathrm{tr}(\mathbf{D}^2)]^{1/2}, \quad \tilde{\Omega} = (K/\varepsilon)[-2\mathrm{tr}(\mathbf{W}^2)]^{1/2}$$

and $\beta_1 = -0.4\tilde{C}_\mu$, $\beta_2 = 0.4\tilde{C}_\mu$, $\beta_3 = -1.04\tilde{C}_\mu$, $\gamma_1 = \gamma_2 = 40.0\tilde{C}_\mu^3$, $\gamma_3 = 0$, and $\gamma_4 = -80.0\,\tilde{C}_\mu^3$. Note that, since $\gamma_3 = 0$, the cubic term with $(\mathbf{W}^2\mathbf{D} + \mathbf{D}\mathbf{W}^2)$ in fact makes no contribution to the numerical simulations.

(7) The non-linear cubic $K$–$\varepsilon$ model of Shih *et al.* [8]:

$$\begin{aligned}\boldsymbol{\tau} = {} & \frac{2K}{3}\mathbf{1} - 2\mu_T\mathbf{D} - A_3\frac{K^3}{\varepsilon^2}[\mathbf{DW} - \mathbf{WD}] \\ & + 2A_5\frac{K^4}{\varepsilon^3}\left[\mathbf{WD}^2 - \mathbf{D}^2\mathbf{W} + \mathbf{WDW} - \frac{1}{3}\mathrm{tr}(\mathbf{WDW})\mathbf{1} - \frac{1}{2}(\mathrm{tr}\,\mathbf{D}^2)\mathbf{D}\right] \end{aligned} \tag{21}$$

 

where the coefficients

$$\mu_T = C_\mu f_\mu \frac{K^2}{\varepsilon}, \quad A_3 = \frac{\sqrt{1 - \frac{9}{2}C_\mu^2\left(\frac{KS^*}{\varepsilon}\right)^2}}{0.5 + \frac{3}{2}\frac{K^3}{\varepsilon^2}\Omega^* S^*}, \quad A_5 = \frac{1.6\mu_T}{\frac{K^4}{\varepsilon^3}\frac{7\mathrm{tr}\,\mathbf{D}^2 + \mathrm{tr}\,\mathbf{W}^2}{4}}$$

in which $C_\mu = \frac{1}{4.0 + A_s(KU^*/\varepsilon)}$, $f_\mu = [1 - \exp(-a_1 R_K - a_3 R_K^3 - a_5 R_K^5)]^{1/2}$, $A_s = \sqrt{6}\cos\phi$, $\phi = \frac{1}{3}\arccos(\sqrt{6}\mathrm{tr}\,\mathbf{D}^3/(\sqrt{\mathrm{tr}\,\mathbf{D}^2}\,)^3)$, $U^* = \sqrt{\mathrm{tr}\,\mathbf{D}^2 + \mathrm{tr}\,\mathbf{W}^2}$, $a_1 = 1.7 * 10^{-3}$, $a_3 = 1 * 10^{-9}$, $a_5 = 5 * 10^{-10}$, and $R_K = \sqrt{K}\,y/\nu$. Note that here the coefficient $A_5$ appearing in the cubic term was identified based on the experimental data of fully-developed rotating pipe flow.

(8) The non-linear cubic $K$–$\varepsilon$ model of Huang and Ma [16]:

$$\begin{aligned}\boldsymbol{\tau} = {} & \frac{2K}{3}\mathbf{1} - 2C_\mu\frac{K^2}{\varepsilon}\mathbf{D} + \gamma_1 C_\mu^2\frac{K^3}{\varepsilon^2}\left[\mathbf{D}^2 - \frac{1}{3}\mathrm{tr}(\mathbf{D}^2)\mathbf{1}\right] - \gamma_2 C_\mu^2\frac{K^3}{\varepsilon^2}\overset{\circ}{\mathbf{D}} - \gamma_3 C_\mu\frac{K^2}{\varepsilon^3}(K\dot{\varepsilon} - 2\dot{K}\varepsilon)\mathbf{D} \\ & + \gamma_4 C_\mu^2\frac{K^3}{\varepsilon^2}\left[\mathbf{W}^2 - \frac{1}{3}\mathrm{tr}(\mathbf{W}^2)\mathbf{1}\right] + \gamma_5 C_\mu^2\frac{K^3}{\varepsilon^2}[\mathbf{DW} - \mathbf{WD}] - \gamma_6 C_\mu^3\frac{K^4}{\varepsilon^3}[\overset{\circ}{\mathbf{D}}\mathbf{W} - \mathbf{W}\overset{\circ}{\mathbf{D}}] \\ & - \gamma_7 C_\mu\frac{K^4}{\varepsilon^3}\left[\mathbf{D}\overset{\circ}{\mathbf{D}} + \overset{\circ}{\mathbf{D}}\mathbf{D} - \frac{2}{3}\mathrm{tr}(\mathbf{D}\overset{\circ}{\mathbf{D}})\mathbf{1}\right] \end{aligned} \tag{22}$$

where $C_\mu = 0.09$, $\gamma_1 = 2.896$, $\gamma_2 = 2.784$, $\gamma_3 = 0.843$, $\gamma_4 = 0.8482$, $\gamma_5 = 0.6344$, $\gamma_6 = 0.7767$, and $\gamma_7 = 0.6885$. The coefficients $\gamma_1, \ldots, \gamma_6$ were identified based on the experimental results of homogeneous turbulent shear flow of Tavoularis and Corrsin [23] (see References [16, 19]); and the coefficient $\gamma_7$ of the last term in Equation (22), a term in the same form as that in the CLS model, is determined in this work by making use of the experimental data of Imao *et al.* [6]. For simplicity in notation and without confusion, hereinafter, an overdot ( $\dot{}$ ) is also used to denote the material time derivative associated with the mean velocity $\bar{\mathbf{v}}$, i.e. $D/Dt$, e.g. $(D/Dt)K = \dot{K} = (\partial/\partial t)K + (\mathrm{grad}\,K)\cdot\bar{\mathbf{v}}$. Here, $\overset{\circ}{\mathbf{D}} = (D/Dt)\mathbf{D} + \mathbf{DW} - \mathbf{WD}$ is the Jaumann derivative of the mean stretching tensor $\mathbf{D}$.

It is seen from Equations (1) and (3) that only $\tau_{r\theta}$ and $\tau_{rz}$ contribute to the modelling of the mean swirl velocity $U_\theta(r)$ and the mean axial velocity $U_z(r)$, respectively. After a bit cumbersome but straightforward algebra, we obtain:

For the model of Craft *et al.* (CLS) [15], there are

$$\begin{aligned}\tau_{r\theta} = {} & \left[-2\tilde{C}_\mu\frac{K^2}{\varepsilon} + \gamma_1\frac{K^4}{\varepsilon^3}(\mathrm{tr}\,\mathbf{D}^2) + \gamma_2\frac{K^4}{\varepsilon^3}(\mathrm{tr}\,\mathbf{W}^2)\right]D_{r\theta} - \gamma_4\frac{K^4}{\varepsilon^3}(\mathbf{WD}^2 - \mathbf{D}^2\mathbf{W})_{r\theta} \\ = {} & \frac{1}{2}\left[-2\tilde{C}_\mu\frac{K^2}{\varepsilon} + \frac{1}{2}\gamma_1\frac{K^4}{\varepsilon^3}\left\{\left(\frac{\mathrm{d}U_\theta}{\mathrm{d}r} - \frac{U_\theta}{r}\right)^2 + \left(\frac{\mathrm{d}U_z}{\mathrm{d}r}\right)^2\right\} - \frac{1}{2}\gamma_2\frac{K^4}{\varepsilon^3}\left\{\left(\frac{\mathrm{d}U_\theta}{\mathrm{d}r} + \frac{U_\theta}{r}\right)^2\right. \right. \\ & \left.\left. + \left(\frac{\mathrm{d}U_z}{\mathrm{d}r}\right)^2\right\}\right]\left(\frac{\mathrm{d}U_\theta}{\mathrm{d}r} - \frac{U_\theta}{r}\right) - \frac{1}{4}\gamma_4\frac{K^4}{\varepsilon^3}\left(\frac{U_\theta}{r}\right)\left(\frac{\mathrm{d}U_z}{\mathrm{d}r}\right)^2 \end{aligned} \tag{23}$$

 

$$\tau_{rz} = \left[-2\tilde{C}_\mu \frac{K^2}{\varepsilon} + \gamma_1 \frac{K^4}{\varepsilon^3}(\mathrm{tr}\,\mathbf{D}^2) + \gamma_2 \frac{K^4}{\varepsilon^3}(\mathrm{tr}\,\mathbf{W}^2)\right] D_{rz} - \gamma_4 \frac{K^4}{\varepsilon^3}(\mathbf{WD}^2 - \mathbf{D}^2\mathbf{W})_{rz}$$

$$= \frac{1}{2}\left[-2\tilde{C}_\mu \frac{K^2}{\varepsilon} + \frac{1}{2}\gamma_1 \frac{K^4}{\varepsilon^3}\left\{\left(\frac{\mathrm{d}U_\theta}{\mathrm{d}r} - \frac{U_\theta}{r}\right)^2 + \left(\frac{\mathrm{d}U_z}{\mathrm{d}r}\right)^2\right\} - \frac{1}{2}\gamma_2 \frac{K^4}{\varepsilon^3}\left\{\left(\frac{\mathrm{d}U_\theta}{\mathrm{d}r} + \frac{U_\theta}{r}\right)^2 + \left(\frac{\mathrm{d}U_z}{\mathrm{d}r}\right)^2\right\}\right]\left(\frac{\mathrm{d}U_z}{\mathrm{d}z}\right) - \frac{1}{4}\gamma_4 \frac{K^4}{\varepsilon^3}\left(\frac{U_\theta}{r}\right)\left(\frac{\mathrm{d}U_z}{\mathrm{d}r}\right)\left(\frac{U_\theta}{r} - \frac{\mathrm{d}U_\theta}{\mathrm{d}r}\right) \tag{24}$$

For the model of Shih *et al.* [8], we have

$$\tau_{r\theta} = -2\mu_T D_{r\theta} - A_5 \frac{K^4}{\varepsilon^3}(\mathrm{tr}\,\mathbf{D}^2) D_{r\theta} + 2A_5 \frac{K^4}{\varepsilon^3}(\mathbf{WD}^2 - \mathbf{D}^2\mathbf{W} + \mathbf{WDW})_{r\theta}$$

$$= -\left\{\mu_T + \frac{A_5}{4}\frac{K^4}{\varepsilon^3}\left[\left(\frac{\mathrm{d}U_\theta}{\mathrm{d}r}\right)^2 - 2\left(\frac{\mathrm{d}U_\theta}{\mathrm{d}r}\right)\left(\frac{U_\theta}{r}\right) + \left(\frac{U_\theta}{r}\right)^2 + \left(\frac{\mathrm{d}U_z}{\mathrm{d}r}\right)^2\right]\right\}\left(\frac{\mathrm{d}U_\theta}{\mathrm{d}r} - \frac{U_\theta}{r}\right)$$

$$+ \frac{1}{4}A_5 \frac{K^4}{\varepsilon^3}\left[\left(\frac{\mathrm{d}U_\theta}{\mathrm{d}r}\right)^3 + \left(\frac{\mathrm{d}U_\theta}{\mathrm{d}r}\right)^2\left(\frac{U_\theta}{r}\right) - \left(\frac{\mathrm{d}U_\theta}{\mathrm{d}r}\right)\left(\frac{U_\theta}{r}\right)^2 - \left(\frac{U_\theta}{r}\right)^3 + \left(\frac{\mathrm{d}U_\theta}{\mathrm{d}r}\right)\left(\frac{\mathrm{d}U_z}{\mathrm{d}r}\right)^2 + 3\left(\frac{U_\theta}{r}\right)\left(\frac{\mathrm{d}U_z}{\mathrm{d}r}\right)^2\right]$$

$$= -\mu_T\left(\frac{\mathrm{d}U_\theta}{\mathrm{d}r} - \frac{U_\theta}{r}\right) + A_5 \frac{K^4}{\varepsilon^3}\left[\left(\frac{U_\theta}{r}\right)\left(\frac{\mathrm{d}U_z}{\mathrm{d}r}\right)^2 - \left(\frac{\mathrm{d}U_\theta}{\mathrm{d}r}\right)\left(\frac{U_\theta}{r}\right)^2 + \left(\frac{\mathrm{d}U_\theta}{\mathrm{d}r}\right)^2\left(\frac{U_\theta}{r}\right)\right] \tag{25}$$

$$\tau_{rz} = -2\mu_T D_{rz} - A_5 \frac{K^4}{\varepsilon^3}(\mathrm{tr}\,\mathbf{D}^2) D_{rz} + 2A_5 \frac{K^4}{\varepsilon^3}(\mathbf{WD}^2 - \mathbf{D}^2\mathbf{W} + \mathbf{WDW})_{rz}$$

$$= -\left\{\mu_T + \frac{A_5}{4}\frac{K^4}{\varepsilon^3}\left[\left(\frac{\mathrm{d}U_\theta}{\mathrm{d}r}\right)^2 - 2\left(\frac{\mathrm{d}U_\theta}{\mathrm{d}r}\right)\left(\frac{U_\theta}{r}\right) + \left(\frac{U_\theta}{r}\right)^2 + \left(\frac{\mathrm{d}U_z}{\mathrm{d}r}\right)^2\right]\right\}\left(\frac{\mathrm{d}U_z}{\mathrm{d}r}\right)$$

$$+ \frac{1}{4}A_5 \frac{K^4}{\varepsilon^3}\left[\left(\frac{U_\theta}{r}\right)^2\left(\frac{\mathrm{d}U_z}{\mathrm{d}r}\right) - 2\left(\frac{\mathrm{d}U_\theta}{\mathrm{d}r}\right)\left(\frac{U_\theta}{r}\right)\left(\frac{\mathrm{d}U_z}{\mathrm{d}r}\right) + \left(\frac{\mathrm{d}U_\theta}{\mathrm{d}r}\right)^2\left(\frac{\mathrm{d}U_z}{\mathrm{d}r}\right) + \left(\frac{\mathrm{d}U_z}{\mathrm{d}r}\right)^3\right]$$

$$= -\mu_T\left(\frac{\mathrm{d}U_z}{\mathrm{d}r}\right) \tag{26}$$

 

And, for the model of Huang and Ma [16], abbreviated to HM model hereinafter (note that in this case $(\dot{\mathbf{D}})_{r\theta}=(\dot{\mathbf{D}})_{rz}=\dot{K}=\dot{\varepsilon}=0$), we arrive at

$$\begin{aligned}\tau_{r\theta} &= -2C_\mu\frac{K^2}{\varepsilon}D_{r\theta}-\gamma_6C_\mu^3\frac{K^4}{\varepsilon^3}[\mathring{\mathbf{D}}\mathbf{W}-\mathbf{W}\mathring{\mathbf{D}}]_{r\theta}-\gamma_7C_\mu^3\frac{K^4}{\varepsilon^3}\left[\mathbf{D}\mathring{\mathbf{D}}+\mathring{\mathbf{D}}\mathbf{D}-\frac{2}{3}\mathrm{tr}(\mathbf{D}\mathring{\mathbf{D}})\mathbf{1}\right]_{r\theta}\\ &= -2C_\mu\frac{K^2}{\varepsilon}D_{r\theta}-\gamma_6C_\mu^3\frac{K^4}{\varepsilon^3}[\mathbf{D}\mathbf{W}^2-2\mathbf{W}\mathbf{D}\mathbf{W}+\mathbf{W}^2\mathbf{D}]_{r\theta}-\gamma_7C_\mu^3\frac{K^4}{\varepsilon^3}[\mathbf{D}^2\mathbf{W}-\mathbf{W}\mathbf{D}^2]_{r\theta}\\ &= -C_\mu\frac{K^2}{\varepsilon}\left(\frac{\mathrm{d}U_\theta}{\mathrm{d}r}-\frac{U_\theta}{r}\right)+\frac{1}{2}\gamma_6C_\mu^3\frac{K^4}{\varepsilon^3}\left[\left(\frac{\mathrm{d}U_\theta}{\mathrm{d}r}\right)^3+\left(\frac{\mathrm{d}U_\theta}{\mathrm{d}r}\right)^2\left(\frac{U_\theta}{r}\right)-\left(\frac{\mathrm{d}U_\theta}{\mathrm{d}r}\right)\left(\frac{U_\theta}{r}\right)^2\right.\\ &\quad\left.-\left(\frac{U_\theta}{r}\right)^3+\left(\frac{\mathrm{d}U_\theta}{\mathrm{d}r}\right)\left(\frac{\mathrm{d}U_z}{\mathrm{d}r}\right)^2+\frac{1}{2}\left(\frac{U_\theta}{r}\right)\left(\frac{\mathrm{d}U_z}{\mathrm{d}r}\right)^2\right]+\frac{1}{4}\gamma_7C_\mu^3\frac{K^4}{\varepsilon^3}\left(\frac{U_\theta}{r}\right)\left(\frac{\mathrm{d}U_z}{\mathrm{d}r}\right)^2 \qquad (27)\end{aligned}$$

$$\begin{aligned}\tau_{rz} &= -2C_\mu\frac{K^2}{\varepsilon}D_{rz}-\gamma_6C_\mu^3\frac{K^4}{\varepsilon^3}[\mathring{\mathbf{D}}\mathbf{W}-\mathbf{W}\mathring{\mathbf{D}}]_{rz}-\gamma_7C_\mu^3\frac{K^4}{\varepsilon^3}\left[\mathbf{D}\mathring{\mathbf{D}}+\mathring{\mathbf{D}}\mathbf{D}-\frac{2}{3}\mathrm{tr}(\mathbf{D}\mathring{\mathbf{D}})\mathbf{1}\right]_{rz}\\ &= -2C_\mu\frac{K^2}{\varepsilon}D_{rz}-\gamma_6C_\mu^3\frac{K^4}{\varepsilon^3}[\mathbf{D}\mathbf{W}^2-2\mathbf{W}\mathbf{D}\mathbf{W}+\mathbf{W}^2\mathbf{D}]_{rz}-\gamma_7C_\mu^3\frac{K^4}{\varepsilon^3}[\mathbf{D}^2\mathbf{W}-\mathbf{W}\mathbf{D}^2]_{rz}\\ &= -C_\mu\frac{K^2}{\varepsilon}\left(\frac{\mathrm{d}U_z}{\mathrm{d}r}\right)-\frac{1}{4}\gamma_6C_\mu^3\frac{K^4}{\varepsilon^3}\left(\frac{\mathrm{d}U_z}{\mathrm{d}r}\right)\left[\left(\frac{U_\theta}{r}\right)^2-2\left(\frac{\mathrm{d}U_\theta}{\mathrm{d}r}\right)^2-2\left(\frac{\mathrm{d}U_z}{\mathrm{d}r}\right)^2\right.\\ &\quad\left.-\left(\frac{\mathrm{d}U_\theta}{\mathrm{d}r}\right)\left(\frac{U_\theta}{r}\right)\right]-\frac{1}{4}\gamma_7C_\mu^3\frac{K^4}{\varepsilon^3}\left(\frac{U_\theta}{r}\right)\left(\frac{\mathrm{d}U_z}{\mathrm{d}r}\right)\left[\left(\frac{\mathrm{d}U_\theta}{\mathrm{d}r}\right)-\left(\frac{U_\theta}{r}\right)\right] \qquad (28)\end{aligned}$$

Obviously, the cubic terms appearing in the above three models play a key role in predicting the mean swirl velocity $U_\theta$—indeed, neglecting them will lead to the same solid-body-rotation mean swirl velocity $U_\theta$ as predicted by the standard $K$–$\varepsilon$ model. Moreover, it is interesting to see that these cubic terms in Equations (23), (25), and (27) now actually combine the *linear terms* in each model, respectively, as a whole, to predict the mean swirl velocity $U_\theta$.

Let us compare the contributing cubic terms appearing in the above three cubic models.

The cubic terms (implicit and explicit) in the CLS model:

$$\left[\gamma_1\frac{K^4}{\varepsilon^3}(\mathrm{tr}\,\mathbf{D}^2)+\gamma_2\frac{K^4}{\varepsilon^3}(\mathrm{tr}\,\mathbf{W}^2)\right]\mathbf{D}-\gamma_4\frac{K^4}{\varepsilon^3}(\mathbf{W}\mathbf{D}^2-\mathbf{D}^2\mathbf{W}) \qquad (29)$$

The cubic terms (implicit and explicit) in the model of Shih *et al.* [8]:

$$-A_5\frac{K^4}{\varepsilon^3}(\mathrm{tr}\,\mathbf{D}^2)\mathbf{D}+2A_5\frac{K^4}{\varepsilon^3}(\mathbf{W}\mathbf{D}^2-\mathbf{D}^2\mathbf{W}+\mathbf{W}\mathbf{D}\mathbf{W}) \qquad (30)$$

The cubic terms (explicit) in the HM model:

$$-\gamma_6C_\mu^3\frac{K^4}{\varepsilon^3}[\mathbf{D}\mathbf{W}^2-2\mathbf{W}\mathbf{D}\mathbf{W}+\mathbf{W}^2\mathbf{D}]-\gamma_7C_\mu^3\frac{K^4}{\varepsilon^3}[\mathbf{D}^2\mathbf{W}-\mathbf{W}\mathbf{D}^2] \qquad (31)$$

 

A comparison of the above three equations indicates that the HM model contains more cubic terms involving the mean spin tensor $\mathbf{W}$ and its interaction with the mean stretching tensor $\mathbf{D}$ than the CLS model and the model of Shih *et al.* [8]. Moreover, it is seen from Equations (24) and (28) that, in both the CLS model and the HM model, the cubic terms in each model make a direct contribution to modelling the rotation effect of the mean axial velocity $U_z$, whereas the cubic terms in the model of Shih *et al.* [8] make no contributions in this regard—in fact, the prediction of $U_z$ based on their model relies on the linear term of the mean strain-rate tensor, i.e. $-2\mu_T D_{rz}$, as seen in Equation (26), in which a generalized eddy viscosity $\mu_T$, being a function of $\mathrm{tr}\,\mathbf{D}^2$ and $\mathrm{tr}\,\mathbf{W}^2$, accounts for some non-linear effects of the mean deformation of turbulence, however.

## 3. NUMERICAL RESULTS AND DISCUSSIONS

### 3.1. Numerical method

In the following, we shall make use of the conventional modelled $K$ equation and $\varepsilon$ equation for numerical calculations, which read, respectively,

$$\dot{K} = -\tau_{ij}\frac{\partial \bar{v}_i}{\partial x_j} - \varepsilon + \frac{\partial}{\partial x_i}\left(\frac{v_T}{\sigma_K}\frac{\partial K}{\partial x_i}\right) + v\nabla^2 K \tag{32}$$

$$\dot{\varepsilon} = -C_{\varepsilon 1}\frac{\varepsilon}{K}\tau_{ij}\frac{\partial \bar{v}_i}{\partial x_j} - C_{\varepsilon 2}\frac{\varepsilon^2}{K} + \frac{\partial}{\partial x_i}\left(\frac{v_T}{\sigma_\varepsilon}\frac{\partial \varepsilon}{\partial x_i}\right) + v\nabla^2 \varepsilon \tag{33}$$

where $v_T = C_\mu K^2/\varepsilon$, $C_\mu = 0.09$, $C_{\varepsilon 1} = 1.44$, $C_{\varepsilon 2} = 1.92$, $\sigma_K = 1.0$, and $\sigma_\varepsilon = 1.3$.

Throughout our numerical calculations, the finite-volume method with non-orthogonal grids has been used; variable storage is co-located and cell-centred, with Rhie–Chow interpolation for cell-face mass fluxes (see also References [24, 25]). The SIMPLE pressure-correction algorithm is adopted to obtain the pressure field. The convection terms appearing in all of the equations concerned, e.g. the averaged Navier–Stokes equations, are discretized by a hybrid technique of the first-order upwind scheme and the second-order central differencing scheme, while the diffusion terms are approximated by the second-order central differencing scheme. Here, Stone's strong implicit procedure (SIP) method is used together with the under-relaxation factors. The mean-flow equations and the turbulent transport equations are solved by uncoupled approach. This algorithm has been found to yield rapid convergence to steady state. Convergence is judged by monitoring the magnitude of the absolute residual source of mass and momentum, normalized by the respective inlet fluxes. The iteration is continued until all above residuals fall below 0.05%.

In computation of the wall-bounded turbulent shear flows, for example, the boundary layer flow and the separated flow, it is important to carefully deal with the near-wall turbulence behaviour. Usually, there are two kinds of methods, both of which are popular in practice—one is the so-called wall function, the other is the damping function. In our computations, we have adopted the damping function given in Reference [15]. Moreover, sufficiently fine grids are employed to ensure that $y^+ < 0.5$ along the first grid-line from the wall for the use

 

of the damping function. Our numerical results for the following test cases indicate that the application of the afore-mentioned damping function appears to be successful.

### 3.2. *Test case 1. The fully-developed turbulent flow in an axially rotating pipe*

In this test case, we shall compare our numerical results with the experimental data of Imao *et al.* [6] in their experimental studies of the rotation effects on the turbulent swirling flow induced by the rotating pipe (see the experimental apparatus shown in Figure 1).

Here, the inner diameter $D$ of the pipe is 30 mm. At the entrance of the pipe a uniform axial velocity profile is specified. With the pipe's rotating, the velocity components along the axial, radial, and circumferential directions are gradually developed, and at the location $L = 120D$ the turbulent flow becomes fully-developed. The control parameter of the flow is a non-dimensional rotation rate defined by

$$S = W_{\mathrm{w}}/U_{\mathrm{m}}$$

where $W_{\mathrm{w}}$ is the tangential velocity of the pipe wall, and $U_{\mathrm{m}}$ is the bulk mean axial velocity. In the present numerical computation $S = 0.5$. The Reynolds number based on $U_{\mathrm{m}}$ and $D$ is $2 \times 10^4$. A $200 \times 120$ highly-stretched non-uniform grid has been used in our numerical calculations, ensuring $y^+ < 0.5$ along the first grid-line from the wall.

The computational results for the mean tangential velocity profile are shown in Figure 2. As has been noted in our previous analysis, the numerical simulations clearly indicate that the linear eddy-viscosity turbulence model (SKE) predicts a solid-body-rotation mean tangential velocity and thus fails to correctly describe the rotation effects on the turbulence as observed in experiments. By contrast, all of the three non-linear cubic models produce a parabolic-like tangential velocity profile, in good agreement with the experimental data. It appears that the HM model performs better than the other two cubic models. The mean axial velocity is given in Figure 3. It is seen that the mean axial velocity is not sensitive to the turbulence model. The differences of the results obtained by using different models are not substantial—all the three cubic models agree pretty well with the experimental data. Overall, the HM model outdoes a little bit the other two cubic models, which may be due to the fact that the cubic terms of the model contains more mean spin tensors that represent the interaction between the mean spin tensor **W** and the mean stretching tensor **D**, as mentioned earlier. Note that in addition to the frame-indifferent mean stretching tensor, the frame-dependent mean spin tensor is expected to play an effective role in turbulence modelling at large (see References [16, 26]), which is physically in conformity with the ensemble-averaged Navier–Stokes equations.

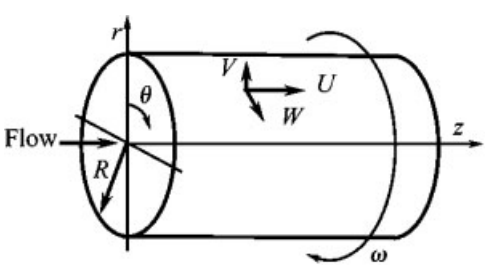


Figure 1. Geometry of the fully-developed rotating pipe flow.

 

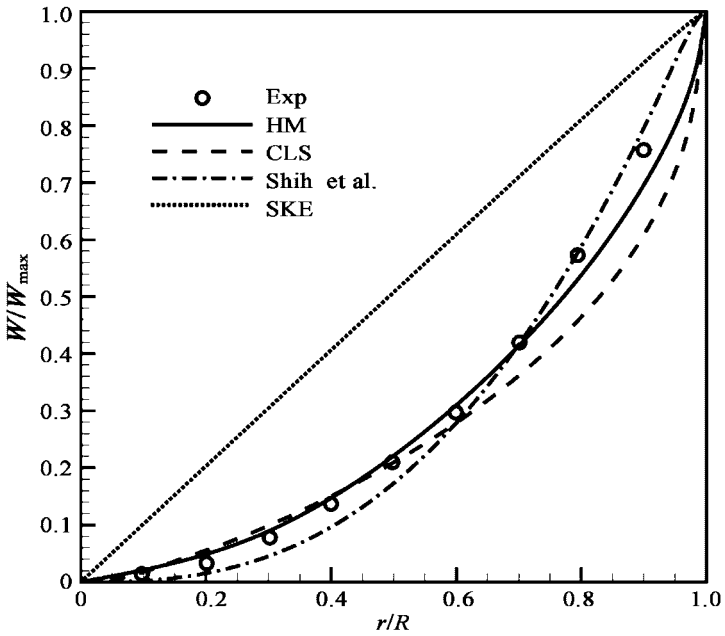


Figure 2. Tangential velocity profile.

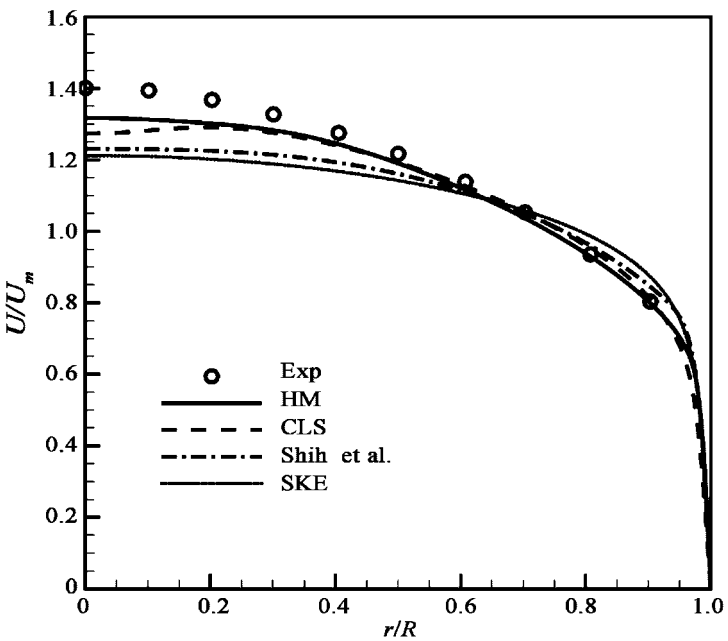


Figure 3. Axial velocity profile.

 

### 3.3. Test case 2. The turbulent swirling flow in an axisymmetric chamber

It is seen from the previous test case that the contributions of the cubic terms in a non-linear cubic $K$–$\varepsilon$ model are significant in predicting the rotation effects on the swirling turbulence. Here, to further assess the performance of these cubic models, we shall carry out numerical simulations for another typical turbulent swirling flow, the swirling flow in an axisymmetric chamber, and make a comparison with the experimental data of Ahmed and Nejad [20]. The flow geometry is shown in Figure 4. The swirling flow produced by the upstream swirler enters the abruptly expanded axisymmetric chamber. The incoming axial velocity of the central line at the entrance is $U_{\text{ref}} = 19.2 \pm 0.4\,\text{m/s}$, based on which and the inner diameter of the chamber the Reynolds number is $1.25 \times 10^5$. The rotation rate is defined as

$$S = \left( \int_0^R UWr^2 \, \mathrm{d}r \right) \Big/ \left( R \int_0^R U^2 r \, \mathrm{d}r \right)$$

where $U$ and $W$ are the axial and tangential velocity respectively and $R$ is the chamber's radius. In the present numerical simulation $S = 0.5$, thus, the rotation effect is not very strong. Here, a $180 \times 120$ highly-stretched non-uniform grid is used, and the grids are densified in the region near the chamber wall and the separated zone. The distance of the first grid line to the wall $y^+$ is smaller than 0.5. The computational condition at the incoming boundary is extrapolated from the experimental data at $x/H = 0.38$ (see Figure 4).

Figure 5 gives the tangential velocity profiles at six horizontal locations: $x/H = 2, 3, 5, 8, 10$, and 15, respectively. It is seen that near the central region around the symmetric axis of the chamber, the tangential velocity obtained by using the HM model is in very good agreement with the experimental data, and correctly predicts the rotation effects on turbulence. The results given by the CLS model and the model of Shih *et al.* [8] do not have a significant advantage over the linear eddy-viscosity model. It is worth noting that the coefficients in both models were calibrated by the experimental data of the fully-developed turbulent flow in a rotating pipe, in which case the rotation effect is dominant while the shear stress is relatively weak—as a result, the rotation effect had been fully estimated and taken into account when determining the model coefficients. By contrast, in the present test case, the rotation effect is not very strong but physically the interaction between the rotation and the shear stress becomes more significant and important—thus, this may partly explain why in this case the results of the CLS model and the model of Shih *et al.* [8] are not as satisfactory as they do in the test case 1

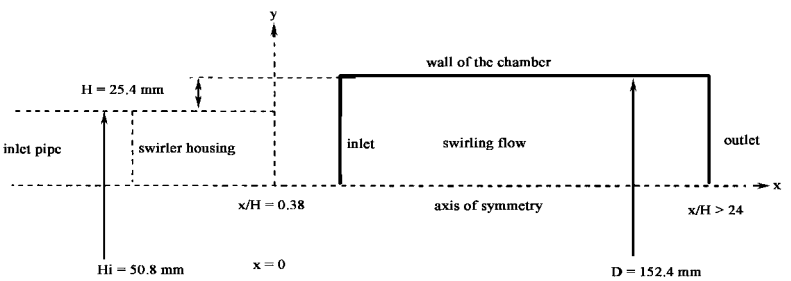


Figure 4. Geometry of the swirling flow in an axisymmetric chamber.

 

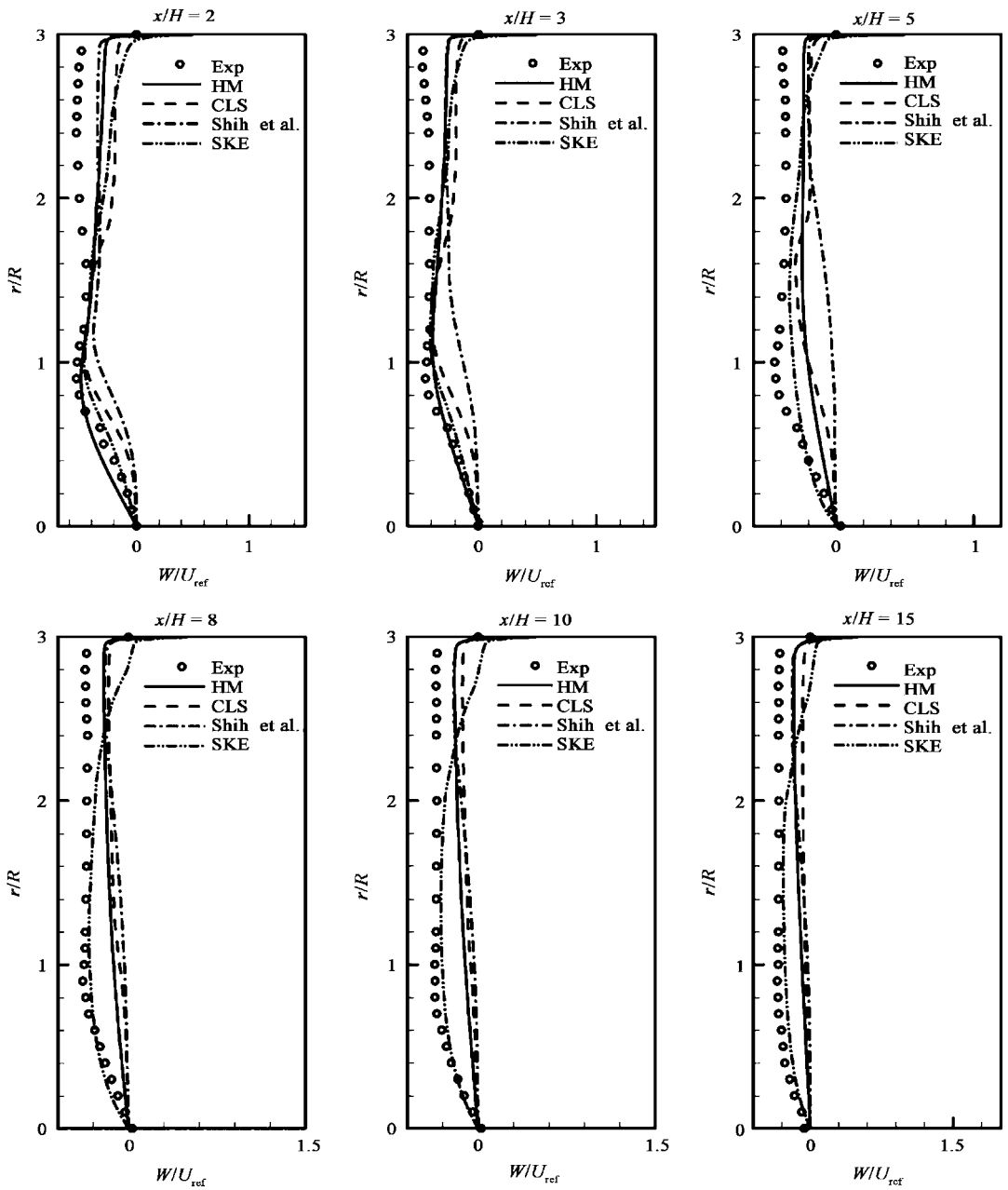


Figure 5. The tangential velocity profile in the axisymmetric chamber.

in which case the rotation effect is dominant. In the region near the chamber wall the flow becomes very complicated because of the influence of the separated vortex near the corner, all of the three cubic models fail to satisfactorily predict the mean velocity distribution, which

 

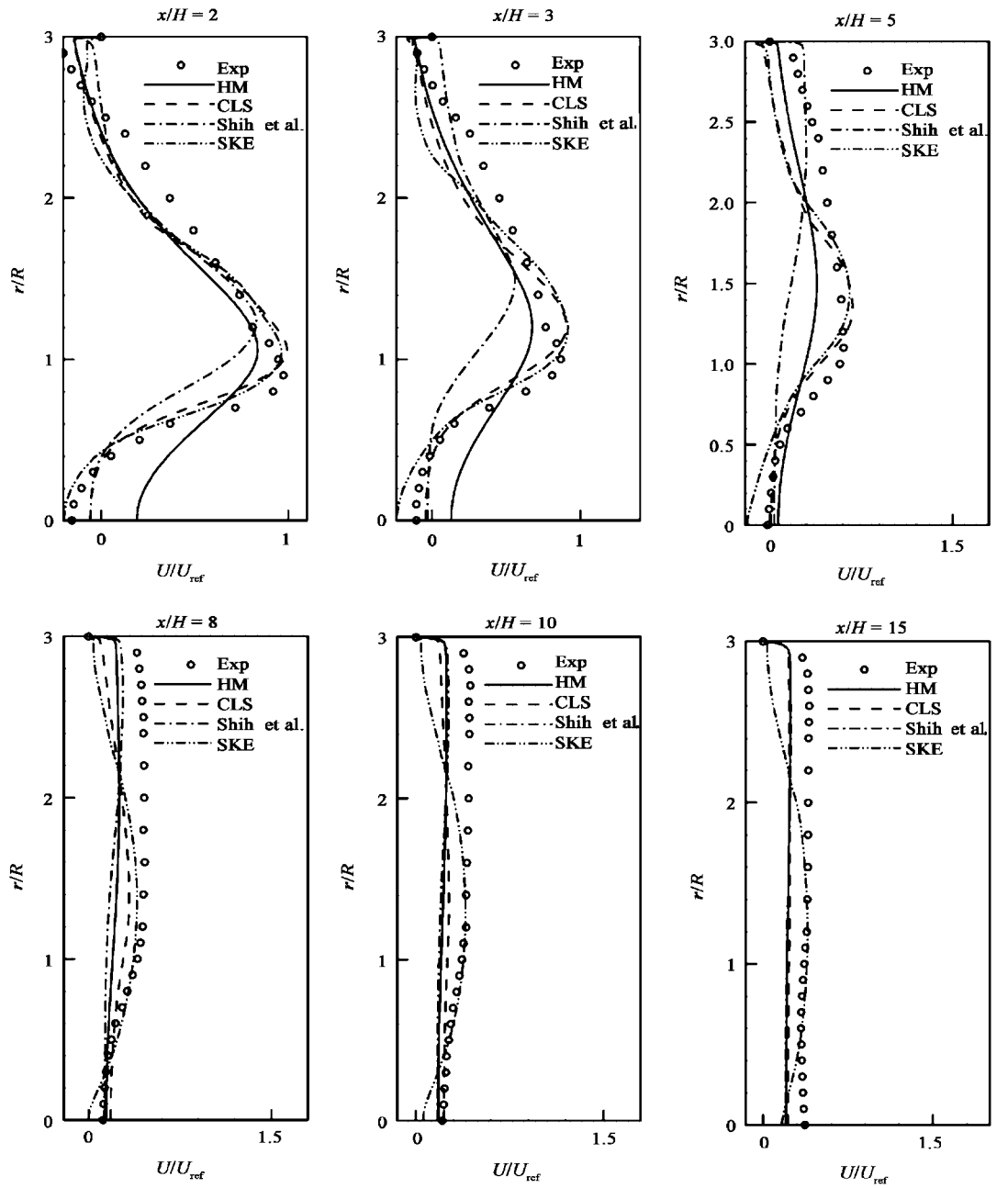


Figure 6. The axial velocity profile in the axisymmetric chamber.

 

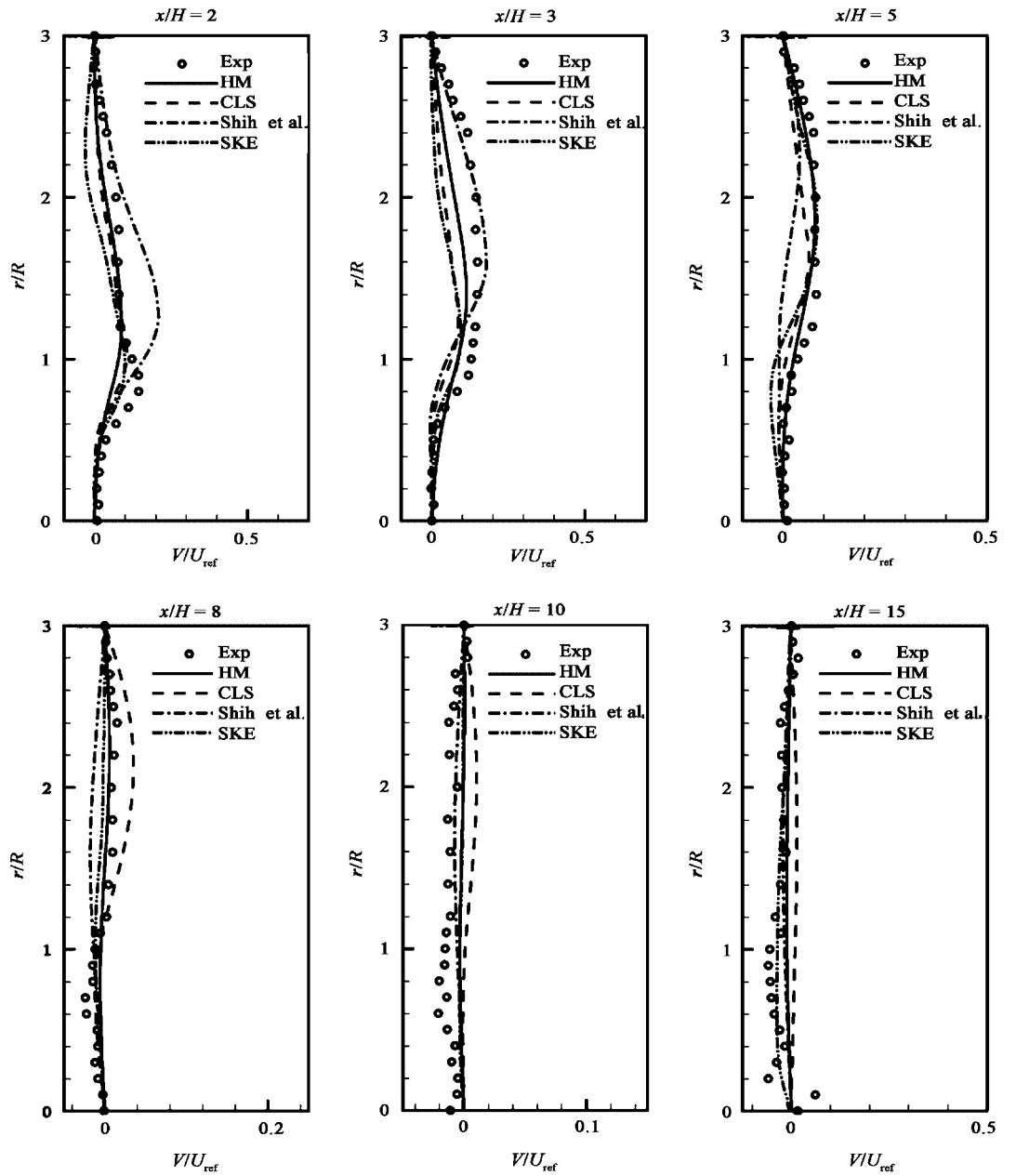


Figure 7. The radial velocity profile in the axisymmetric chamber.

 

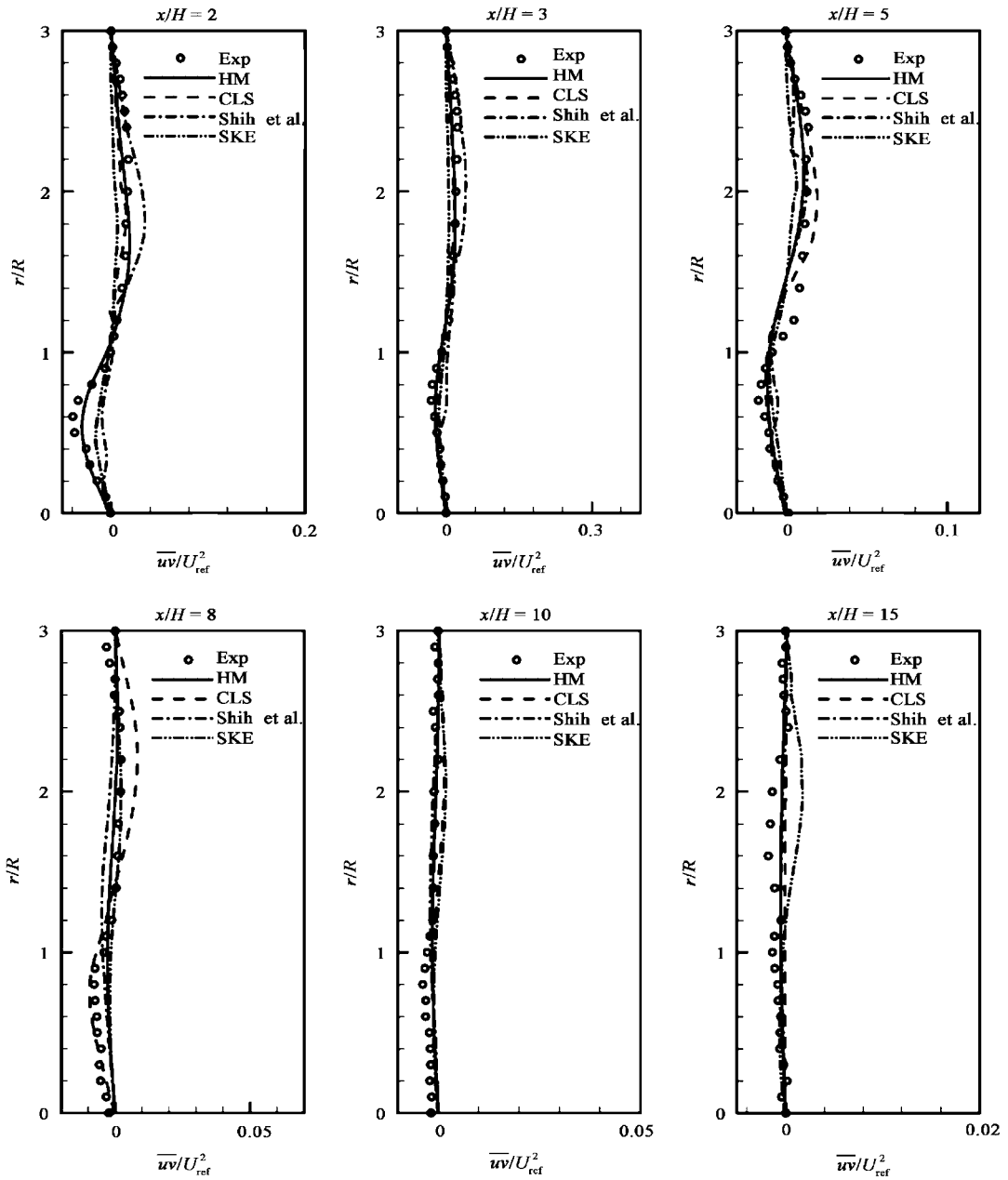


Figure 8. The profile of the Reynolds shear stress.

 

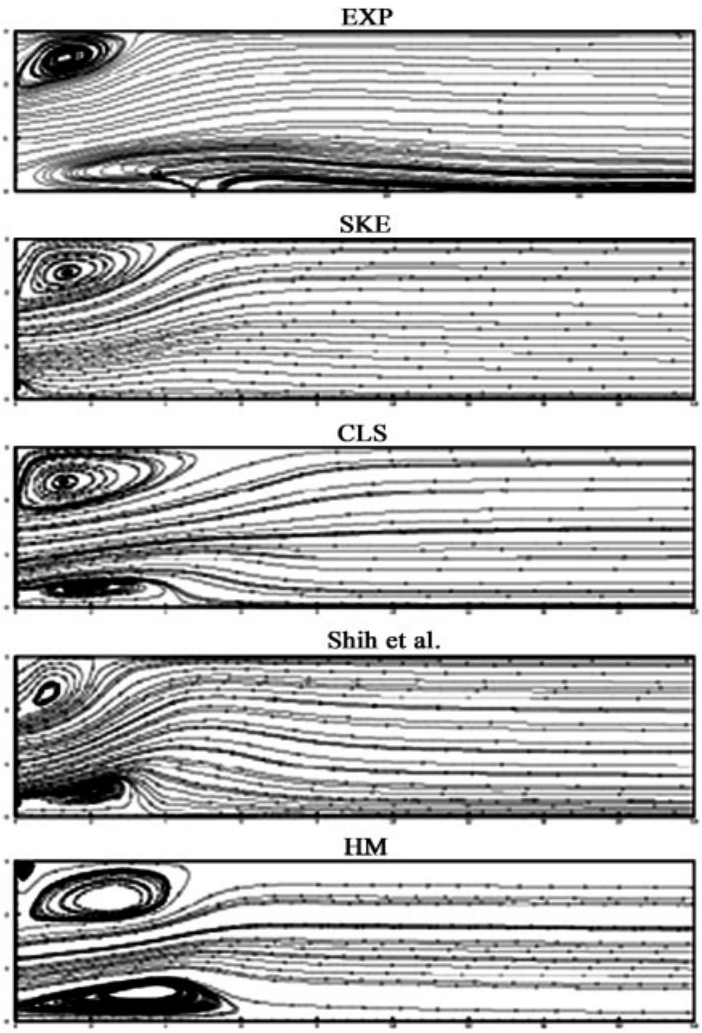


Figure 9. The streamline in the axisymmetric chamber.

may be partly due to the relatively poor performance of the $K$ equation and the $\varepsilon$ equation under this critical situation with the occurrence of flow separation, among other things. In addition, the axial velocity profiles at six locations are presented in Figure 6. It is shown that a recirculation zone is formed near the central region, which is called the free vortex and recognized as a typical characteristic of this kind of swirling flow. It appears that the results given by the HM model are in better agreement with experimental data than the other two cubic models.

For the model of Shih *et al.* [8], near the axis and the wall, the recovery of the mean axial velocity is fast, due to the depression effect of the rotation on turbulence being overestimated. For the HM model, in the region near the wall the shear stress is overestimated, the velocity

 

recovery is slow and, consequently, the computed mean axial velocity becomes smaller than the experimental result.

The mean radial velocity profiles are presented in Figure 7. The model of Shih *et al.* [8] predicts better results for the first three locations, while the CLS model and the HM model perform a bit better in the region of the central part.

The profile of the Reynolds shear stress is shown in Figure 8. Since the magnitude of the Reynolds shear stress is rather small, the differences between the results obtained by using the three cubic models are not very large. In the forced vortex and the free vortex region, the numerical results based on the three cubic models are all better than that obtained by using the linear model.

Finally, the calculated streamline patterns based on four different turbulence models are shown in Figure 9. It is seen that the linear model fails to predict the central recirculation zone. The model of Shih *et al.* [8] underestimates the forced vortex near the corner, due to the velocity recovery being fast and, as a result, the position of the reattachment point is a little bit over-predicted.

## 4. CONCLUDING REMARKS

We have shown that the fully-developed turbulent swirling flow in an axially rotating pipe is by nature a two-point boundary value problem, and the prediction of the rotation effects based on the algebraic two-equation ($K$–$\varepsilon$) modelling approach requires a non-linear cubic model as a necessary condition. The numerical simulations for the fully-developed turbulent swirling flow in an axially rotating pipe and the fully-developed turbulent swirling flow in an axisymmetric chamber using the cubic models of Craft *et al.* [15], Shih *et al.* [8], and Huang and Ma [16] indicate that, in addition to the mean strain-rate tensor, the mean spin tensor actually plays an important role as well. It is interesting to see that the HM model, which employs the Jaumann derivative of the mean stretching tensor, i.e. $\overset{\circ}{\mathbf{D}}$, to account for some history effects of turbulence, yields a number of results better than or comparable to that obtained by using the other two previously proposed cubic models. Moreover, since the coefficients $\gamma_1, \gamma_2, \ldots, \gamma_7$ in the model are functions of the invariants given in Reference [16], it is possible to modify the model with recourse to the experimental and the DNS data concerned so that it can perform better in modelling the complex turbulent flows, noting that the conventional $K$ and $\varepsilon$ equations also need to be appropriately modified so as to better describe the characteristics of the near-wall behaviour of turbulence, like other closure models proposed so far in the literature. It should be noted that the present cubic model has the same number of model coefficients as that in the model of Craft *et al.* [15]; moreover, $\gamma_1$, $\gamma_2, \ldots$ and $\gamma_7$ are all determined based on the experimental data of Tavoularis and Corrsin [23] (see also Reference [16]) and that of Imao *et al.* [6]. Of course, just like all the previously proposed non-linear models, the present model is far from perfect. Nonetheless, we believe that in the near future more and more well-performed models will be developed to better capture the complex phenomena of turbulence. In fact, looking back on the history of the closure problem of turbulence originated from taking the ensemble average on the Navier–Stokes equations, all the past experience of turbulence modelling shows that there doesn't exist a unique or universal closure model for turbulence but rather, ever since Prandtl proposed his

 

pioneering mixing-length model in 1925, a better closure model, one after another, improved yet imperfect, has always been possible to come into play in turbulence modelling.

ACKNOWLEDGEMENTS

This work was supported by the National Natural Science Foundation of China (Grant No. 90205002).

REFERENCES

1. Murakami M, Kikuyama K. Turbulent flow in an axially rotating pipe. *Journal of Fluids Engineering* 1980; **102**:97–103.
2. Kikuyama K, Murakami M, Nishibori K. Development of three-dimensional turbulent boundary layer in an axially rotating pipe. *Journal of Fluids Engineering* 1983; **105**:154–160.
3. Anwer M, So RMC. Rotation effects on a fully-developed tubulent pipe flow. *Experiments in Fluids* 1989; **8**:33–40.
4. Reich G, Beer H. Fluid flow and heat transfer in an axially rotating pipe—I. Effect of rotation on turbulent pipe flow. *International Journal of Fluids Engineering* 1989; **32**:551–561.
5. Kitoh O. Experimental study of turbulent swirling flow in a straight pipe. *Journal of Fluid Mechanics* 1991; **225**:445–479.
6. Imao S, Itoh M, Harada T. Turbulent characteristics of the flow in an axially rotating pipe. *International Journal of Heat and Fluid Flow* 1996; **17**:444–451.
7. Marlin MR, Younis BA. The prediction of turbulent transport in an axially rotating pipe. *International Communications in Heat and Mass Transfer* 1997; **24**:89–98.
8. Shih TH, Zhu J, Liou W, Chen KH, Liu NS, Lumley JL. Modeling of turbulent swirling flows. *Proceedings of 11th Symposium on Turbulent Shear Flows*, Grenoble, France, 1997; 31.1–31.6.
9. Pettersson BA, Andersson HI, Brunvoll AS. Modelling near-wall effects in axially rotating pipe by elliptic relaxation. *AIAA Journal* 1998; **36**:1164–1170.
10. Speziale CG, Younis BA, Berger SA. Analysis and modelling of turbulent flow in an axially rotating pipe. *Journal of Fluid Mechanics* 2000; **407**:1–26.
11. Wallin S, Johansson AV. An explicit algebraic Reynolds stress model for incompressible and compressible turbulent flows. *Journal of Fluid Mechanics* 2000; **403**:89–132.
12. Orlandi P, Fatica M. Direct simulations of turbulent flow in a pipe rotating about its axis. *Journal of Fluid Mechanics* 1997; **343**:43–72.
13. Shih TH, Zhu J, Lumley JL. A new Reynolds stress algebraic equation model. *Computer Methods in Applied Mechanics and Engineering* 1995; **125**:287–302.
14. Launder BE. An introduction to single-point closure methodology. *Proceedings of ERCOFTAC/IUTAM Summer School*, Stockholm, 12–20 June 1995.
15. Craft TJ, Launder BE, Suga K. Development and application of a cubic eddy-viscosity model of turbulence. *International Journal of Heat and Fluid Flow* 1996; **17**:108–115.
16. Huang YN, Ma HY. Reynolds stress model involving the mean spin tensor. *Physical Review E* 2004; **70**:036302.
17. Yoshizawa A, Nisizima S. A non-equilibrium representation of the turbulent viscosity based on a two-scale turbulence theory. *Physics of Fluids A* 1993; **5**:3302–3304.
18. Speziale CG. On non-linear $K$–$l$ and $K$–$\varepsilon$ models of turbulence. *Journal of Fluid Mechanics* 1987; **178**: 459–475.
19. Huang YN. On modelling the Reynolds stress in the context of continuum mechanics. *Communications in Nonlinear Science and Numerical Simulation* 2004; **9**:543–559.
20. Ahmed SA, Nejad AS. Swirling effects on confined flows in axisymmetric geometry. *Journal of Propulsion and Power* 1992; **18**:339–364.
21. Launder BE, Spalding DB. The numerical computation of turbulent flow. *Computer Methods in Applied Mechanics and Engineering* 1974; **3**:269–289.
22. Fu S, Launder BE, Tselipedakis DP. Accommodating the effects of high strain rates in modelling the pressure-strain correlation. Mechanical Engineering Department, UMIST, TR TFD/87/5, March 1987.
23. Tavoularis S, Corrsin S. Experiments in nearly homogeneous turbulent shear flow with a uniform mean temperature gradient. Parts 1 and 2. *Journal of Fluid Mechanics* 1981; **104**:311–367.
24. Ferziger JH, Perić M. *Computational Methods for Fluid Dynamics*, Chapter 7. Springer: Berlin, 1996.
25. Yang XD, Ma HY. Linear and non-linear eddy-viscosity turbulence models for a confined swirling co-axial jet. *Numerical Heat Transfer*, *Part B* 2003; **43**:289–305.
26. Huang YN, Durst F. Reynolds stress under a change of frame of reference. *Physical Review E* 2001; **63**:056305.

 